Assessment of θ-projection concept and fracture cavitation

A. Baldan · E. Tascioglu

Abstract The empirical approach to creep, termed θ-projection concept, is applied to the constant-load data of conventionally cast nickel-base superalloy IN-100 at constant temperature (900 °C). The normal creep curves, obtained at various initial stresses ($\sigma_A = 200-400$ MPa), could be accurately represented by this concept. The change in creep curve shape with stress from tertiary dominated to primary dominated view is presented by the change in the ratio of primary (ε_p) and tertiary strain (ε_t) components to rupture strain (ε_R). It is predicted that failure in the present creep conditions is dominated by the GB cavitation and the growth of the cavities is controlled by the coupled GB diffusion and power-law creep mechanism. In an attempt to provide a physical significance to θ-parameters, it is found that the internal structural variable theory and continuous GB cavitation account well, with suitable assumptions, for the θ description of primary and tertiary creep curves, respectively.

Introduction

In the case where the many metallic components of engineering plants are subjected to creep conditions (i.e. high temperature and stress), creep data equal to the design life are required. When designing materials for high-temperature service the design criteria for long-term operation must guarantee that creep deformation should not cause excessive distortion over the planned service life and that creep failure should not occur within such a required operating life [1]. Such creep fracture represents an obvious "life-limiting" design consideration since the failure or fracture of major components such as nuclear-powered electricity generating plants and gas turbine aero-engine turbine blades could fail catastrophically. For this reason, studying their ability to predict the time to rupture strain has been the major criterion used to assess creep extrapolation techniques.

The interpolation and extrapolation of creep properties play a major part in the process of design components for high-temperature service. Both metallic and ceramic sections can be allowed to undergo only a limited creep strain and they must not experience rupture within the design life. These life times can be very long (~ 30 years for steam plant) and frequent use must be made of extrapolation from short-term data. There are two factors that make such calculations difficult [2]: (a) First, there is no clear idea of the nature of the extrapolation functions that must be applied and this results in a requirement for long-term creep data with rupture lifetimes close to the design life. Such data are scarce and extremely expensive to collect and, further, inhibit the use of new materials in construction. (b) Second, even when suitable long-term data are available, they contain so much scatter that only order of magnitude estimates of creep life are possible. These problems result in overconservative designs, but even so the lack of understanding of the creep process often results in premature failure, particularly at inhomogeneities such as welds.

Long-term creep tests are expensive and sometimes almost impossible to be performed accurately. Thus the

A. Baldan (✉)
Department of Metallurgical and Materials Engineering, University of Mersin, Ciftlikkoy, Mersin, Turkey
e-mail: abaldan@mersin.edu.tr

E. Tascioglu
Department of Mechanical Engineering, Eastern Mediterranean University, Famagusta, Mersin 10, Turkey

creep life prediction by extrapolating short-term creep data to long-term is of vital importance. Three creep extrapolation techniques for the creep design have been used: (a) the theoretical approach, (b) the practical or parametric approach; various methods of creep life predictions such as the Larson–Miller [3], Sherby–Dorn [4], and Manson–Haferd [5] have been proposed so far. However, it is widely accepted that creep life prediction is limited up to twice the longest tests duration available. Therefore, it was ascertained that both tradational methods in (a) and (b) were inappropriate in the present case because of their non-linear relationships. (c) the θ-projection concept [6]; this new concept not only provides a sound theoretical alternative to tradational mechanistic approaches to creep but also introduces a full constitutive relationship which is ideally suited to modern computer-based methods for high-temperature design [7]. The θ-projection method [8] is a procedure for the interpolation and extrapolation of creep properties some of which may have been obtained from accelerated tests. In contrast to the tradational procedures which permit extrapolation by only a factor of about 3, it appears that factors of 50 or more can be achieved using the θ-Projection Concept [3, 8]. In addition to the normal 4-θ projection technique, the so-called 6-θ approach has also been proposed recently to account for the low-strain materials [9]. The method has been applied to a number of commercially important alloys (i.e. [10, 11]) and ceramics [12, 13] with considerable success.

Two important factors should be taken into account when the short-term creep data are to be extrapolated to long-term [14]: (a) the creep mechanism change and (b) the change in microstructure during creep. As decumanted in deformation-mechanism maps [15], it is widely accepted that the creep mechanism depends on temperature and stress. On the extrapolation of short-term creep data to long-term, the change in creep mechanism may be encountered over the range required. The second problem is the change in microstructures during creep since the commercial creep resistance alloys such as the commercial nickel-based superalloys (i.e. IN-100) are generally strengthened by second-phase particles {γ′, Ni_3 (Al, Ti)}, which are sometimes unstable at testing temperatures. Therefore, even if the change in microstructures is minor in short-term creep, serious errors in creep life prediction could occur due to the noticeable change in microstructures during long-term creep.

Although the deformation mechanisms during the course of creep may be either of dislocation bowing, particle cutting, mechanical or microstructural instability, etc., depending on the material and the test conditions imposed, the final fracture eventually occurs due to the formation, growth and coalescence of cavities to form intergranular cracks. This sort of fracture has been reported for materials

that θ-projection concept has been applied, such as low alloy steel [6, 8], Ni-based superalloy [11], pure copper [16] and Al-alloy [17]. Therefore, the purpose of this study is to investigate the relation between the θ-projection concept and fracture cavitation through the assessment of the physical significance of θ parameters.

Background: the θ-projection technique

The well-defined primary and/or tertiary stages are generally recorded during constant-stress creep tests carried out with metals and alloys [18]. The assumption that the secondary or steady-state creep rate provides a satisfactory characterization of creep behavior then conflicts with the observation that, on improving the sensitivity of the extensometers and strain monitoring system employed during tests carried out with pure copper, the main future noted was the decreased duration of the secondary period [18]. The implication of this result is that, with perfect strain measurement, no secondary period exists, i.e., the secondary rate is merely the ostensible-constant rate found when the decay in creep rate during the primary stage is offset by the acceleration due to tertiary processes.

Therefore, the θ-projection concept allows the creep behavior of materials to be discussed in terms of the processes determining primary and tertiary characteristics rather than in terms of "steady-state" mechanisms as with tradational theoretical approaches [7]. In contrast to the tradational parametric procedures (such as the Larson–Miller technique), the θ-methodology allows the whole creep curve to be extrapolated to design (low) stresses from accelerated (high) stresses. Time to any strain can then be "read off" from such extrapolated creep curves.

The θ-projection method is a three-step process [2]: (a) Step 1 consists of analyzing individual creep curves to estimate θ values. These estimates must be carried out in such a manner as to provide statistical information on the reliability of the derived values. (b) In the Step 2, the variation of θ with testing conditions (i.e., stress and temperature) is described and this stage must include its own statistical analysis. (c) Finally, Step 3 is the prediction stage and it is important that the measures of variability derived in the first two steps are used so that genuine interval estimates of creep properties can be obtained.

The shape of the creep curve is described quantitatively by means of a suitable function of time and other fixed parameters. The exact nature of the function will depend on the material and the testing regime, but in general the creep strain ε_c is given by [2]

$$\varepsilon_c = f\left(t, \theta_1, \theta_2, \ldots, \theta_j, \ldots, \theta_m\right), \tag{1}$$

where t is time and the various θ terms are calculable numerical parameters, the values of which determine the

exact shape of the creep curve. In order to quantify the shape of individual strain/time curves, Eq. 1 must be determined.

The various θ are numerical parameters that can be determined from the experimental (ε, t) points. For a collection of uniaxial creep curves obtained under different testing conditions, the θ_j is then related to various stresses σ and temperatures T through an interpolation function g_j such that [9]

$$f_j(\theta_j) = g_j(\sigma, T, \beta_1, \beta_2, \ldots, \beta_k, \ldots, \beta_p). \tag{2}$$

Here the parameters β_k must be determined by a suitable regrerssion procedure [2] and the set of β parameters will be different for each value of θ_j. Once the parameters θ_j and β_k in Eqs. 1 and 2 are known, it is possible to reconstruct any creep curve at arbitrary conditions of stress and temperature so that the equations form a basis for interpolation and extrapolation. Equations 1 and 2 represent the model equations that describe creep in the θ-projection method [2]. Their form must be firmly based in the micromechanism of the deformation process and this requirement has been discussed elsewhere [8, 19].

The 4-θ-projection concept

Evans et al. [6] have proposed a new creep life prediction method (the θ-projection method), which is based on the creep time law containing four parameters $\theta_j (j = 1-4)$. Once the stress and temperature dependence of θ is determined at higher stresses and temperatures, it is in principle possible to predict the entire creep curve at lower stresses and temperatures. They applied the new method to a 1/2Cr-1/2Mo-1/4V steel and demonstrated that it can predict the minimum creep rates after 30 years from the creep data within 3 months [6].

A very general theory involving the gradual development of hard and soft regions during creep and the movement of dislocations in these regions by glide and recovery processes leads to a kinetic description of primary creep [20] which is essentially first order [8], i.e., the primary creep ($\dot{\varepsilon}_p$) is a linearly decreasing function of the primary creep strain ε_p: similarly, processes such as intergranular damage accumulation and microstructural instability can lead to a tertiary creep rate ($\dot{\varepsilon}_t$) which is strain dependent, so that first-order kinetics for $\dot{\varepsilon}_t$ again results [8] with $\dot{\varepsilon}_t$ being an increasing linear function of the tertiary strain, ε_t. Since the overall creep rate $\dot{\varepsilon}_c$ is the sum of $\dot{\varepsilon}_p$ and $\dot{\varepsilon}_t$, integration of the rate equations gives an overall equation for the variation of creep strain ε_c with time t as

$$\begin{aligned} \varepsilon_c &= f(t, \theta_1, \ldots, \theta_4) = \varepsilon_{tot} - \varepsilon_o \\ &= \theta_1[1 - \exp(-\theta_2 t)] + \theta_3[\exp(\theta_4 t) - 1], \end{aligned} \tag{3}$$

where ε_o is the initial strain on loading and ε_{tot} is the total strain after a time t. The initial strain is the least reliable measurement recorded even when high-precision test methods are adopted because the determination ε_o of relies on just two strain readings taken immediately before and immediately after loading [8]. More satisfactory ε_o data are therefore provided using established constant-strain rate methods. θ_1 and θ_3 act as scaling parameters that control the extent, with respect to strain, of the primary and tertiary stages of creep, θ_2 and θ_4 then determine the curvature of the primary and tertiary periods [6, 8] since increasing θ_2 and θ_4 rapidly increases the deceleration in creep rate during primary creep and the acceleration during tertiary creep. With ε_o determined separately, only the $\varepsilon_{c/t}$ curve is then needed to evaluate the θ parameters in Eq. 3 at any stress and temperature, through the use of the non-linear least-square curve fitting routine which has been detailed elsewhere [8]. Full computational codes have been published which allow the estimation of the 4-θ parameters for a normal creep curve obtained at constant stress and temperature [8].

The first term in the right-hand side of Eq. 3 is to represent the effect of work hardening usually dominant in primary creep and the second term is to describe the acceleration of creep which becomes apparent in the tertiary stage of creep. It is clear that Eq. 3 cannot express steady-state creep rate. However, it appears generally applicable to age-hardened creep resistant alloys because their steady-state creep is usually short if present and sometimes totally absent [14]. Since the fit for each curve is good despite changes in curve shape as the test conditions vary, Eq. 3 can provide a basis for a quantitative description of the curve shape changes with stress and temperature [18].

The dependence of creep curve shape on test conditions can be quantified through the variation of the 4-θ parameters with stress and temperature. At each test temperature, the stress/log θ_i relationships are linear so that, as found for numerous metals and alloys [8, 16], the stress and temperature dependences of the θ terms can be expressed using the following simple expression to relate each $\theta_j (j = 1-4)$ to the accelerated test conditions

$$\mathrm{Log}(\theta_{ij}) = \beta_{i0} + \beta_{i1}\sigma_j + \beta_{i2}T_j + \beta_{i3}\sigma_j T_j, \tag{4}$$

where σ_j is the stress associated with test condition j and T_j is the temperature associated with test condition j ($j = 1$ to m). β_{i0} to β_{i3} are constants that can be estimated using the linear least-squares technique. From a knowledge of these coefficients, Eqs. 3 and 4 may be used to construct creep curves for wide ranges of stress and temperature. Alternatively, the weighted least-squares method can be used to reflect the fact that each θ_{ij} value is only an estimate of its true value. The

weights used must reflect the different uncertainties associated with each θ_{ij} [1]. Each θ_i can then be extrapolated to lower stresses and temperatures by simply substituting the required test conditions into Eq. 4. Let $\tilde{\theta}_{ij}$ represent such extrapolated θ values. It is then possible to use these values to predict a variety of creep properties at close to the operating conditions for a designed material.

The 6-θ-projection concept

It is well known that Eq. 3 is quite good representation of creep curves for materials of moderate and high ductility but it gives a poorer fit at low strains and times [9]. This leads to difficulties in the prediction of very low strain properties but since the mis-specifications are over very rapidly it has virtually no effect on properties such as minimum creep rate and rupture time which occur after considerable deformation. However, for low ductility materials this is not the case and the mis-specifications can lead to poor fits of the model function over the whole of the creep curve. Because the poorly represented early strain is of the same order as the total strain to failure, the model function is clearly inappropriate [9]. Since the θ-projection concept relies on projecting the model function shape to describe the creep curve under unknown conditions, the whole method will fail. As a result, the 4-θ-projection method of creep analysis produces the poorest projections at low strains.

In order to solve the problem of poor projection of the 4-θ-projection method at low strains, Evans [9] has recently developed a modification to the basic curve equation (see Eq. 3). The modification takes the form of two additional-θ terms that allow the initial stages of any creep curve to be modeled more accurately. He claims that the poor projections at low strains could be eliminated. He derived detailed equations together with the parameter estimation procedures. According to him, this new approach gives considerably better descriptions of creep curves. His suggestion to solve this mis-specification should improve the prediction of low-strain properties. A general model function, proposed by Evans [9], suggested for a solution to the mis-specification problem has the same form of Eq. 3:

$$\varepsilon_t = \eta(\theta) = \sum_{i=1}^{q} \theta_{2i-1}[1 - \exp(-\theta_{2i})]. \tag{5}$$

If $\theta_{2i-1} > 0$ and $\theta_{2i} > 0$ the ith term in this series represents a process which has a creep rate that decreases with increasing time (e.g., a normal primary curve). If $\theta_{2i-1} < 0$ and $\theta_{2i} < 0$ the term has a rate that increases with increasing time (e.g., a tertiary process). Although there is no theoretical limit to the value of q, and the degree of fit of the model equation to the experimental data can be made as close as desired by increasing q, there are factors which limit the procedure. Each term in Eq. 5 must be capable of

a theoretical explanation in terms of the micromechanisms governing high temperature creep [9]. Correlation's between the estimated θ_i values is likely to prevent the identification of each and every θ_i value.

Primary and tertiary creeps in particle-hardened creep resisting alloys are known to be well represented by the first and second terms in Eq. 3, so that agreement with experimental observation may be achieved by the inclusion of just one further term. The model equation [9]

$$\varepsilon_t = \theta_1[1 - \exp(-\theta_2 t)] + \theta_3[\exp(\theta_4 t) - 1] \\ + \theta_5[1 - \exp(-\theta_6 t)] \tag{6}$$

may thus be appropriate. Since the order of terms in Eq. 6 is unimportant it is convenient to arrange them in such a way that the first two terms have the same significance [9] as those in Eq. 3. θ_5 and θ_6 are two additional parameters required to improve the fit of the creep curve to the experimental data over the early primary stage [9].

Equation 6 along with Eq. 2 are then used to construct a creep curve at any arbitrary stress σ and temperature T so that interpolation and extrapolation of properties is possible, e.g., to conditions typical of operating components.

In order to proceed with a normal creep projection with the new model equation it is necessary to know the form of Eq. 2 for all 6-θ parameters. It is not yet established whether these will be of the same form as those currently in use (i.e., a general linear variation with stress and temperature, see Eq. 4). When they are known the projection is carried out in the usual way with certain modifications to take into account the more complex form of Eq. 6. Some quantities which could previously be found by analytical means may now need some numerical procedures.

Estimation of θ and β parameters

Creep is highly sensitive to metallurgical structure and even small variations from specimen to specimen become important. Thus, small differences in grain size or in particle distribution and morphology can appreciably affect creep rate and imperfections such as non-metallic inclusions can cause considerable variation in tertiary processes. It is not to be expected that these structural features can be controlled uniformly so it is inevitable that appreciable values of statistical scatters and errors will be observed in creep property estimates [2].

It is now necessary to devise a method that will yield estimates of the expected values of θ. The probability distributions and statistical nature of the strain error are unknown a priori so it is necessary to use an ordinary least squares (OLS) procedure [2]. This estimates the expected values of θ by minimizing the sum of the squares of the differences between the model function and the experimentally observed

strain for all creep points. The analysis of single creep curves is easily programmed for computer calculation [8]. The procedure is first to estimate the θ parameters by a least squares method and then to describe the deviations of individual creep strain points from the fitted curve on the basis of interrelated (autocorrelated) errors. This gives considerable information on the nature of the θ estimates.

Evans [1, 21] has studied the estimation issues of the θ parameters in stochastic form in detail. Estimation of θ_i parameters in Eqs. 3 and 6 requires the use of non-linear optimization algorithms. These algorithms can then choose values for θ_i that either minimize the squared deviations of all the recorded strain values around the fitted creep curve or maximize the joint probability of observing all the recorded strain/time data points, i.e., maximize the so-called likelihood function. If e_t is used to represent the deviation of each strain value from the fitted creep curve, then Evans [1, 21] has expressed Eq. 6 in stochastic form as

$$\varepsilon_t = \tilde{\theta}_1\left[1 - \exp\left(-\tilde{\theta}_2 t\right)\right] + \tilde{\theta}_3\left[\exp\left(\tilde{\theta}_4 t\right) - 1\right] + \tilde{\theta}_5\left[1 - \exp\left(-\tilde{\theta}_6 t\right) - 1\right] + e_t, \tag{7}$$

where $\tilde{\theta}_i$ is an estimate of θ_i. These deviations arise for many reasons. One reason [21] is the mis-specifications issue addressed above where the values for e_t are expected to diminish as q is increased in Eq. 5. This aside, e_t also results from experimental inadequacies such as deficiencies in extensometer design, transducers, and temperature control. These experimental issues also inevitably result in values for e_t being correlated with previous values for e_t. This so-called autocorrelation can be expressed in the following way [1, 21]

$$e_t = \rho e_{t-1} + v_t, \tag{8}$$

where ρ is the first-order autocorrelation coefficients, e_{t-1} is the previously recorded value for e and v_t is an additional error variable that is free of autocorrelation. If such autocorrelation is ignored when using an optimization algorithm to estimate each θ_t, then although the resulting estimates will be unbiased they will be inefficient. That is, the uncertainty or variability associated with each estimate of θ_i will be under estimated [21]. Thus the non-linear least squares approach chooses values for θ_i and ρ such that $\sum_t^n v_t^2$ is minimized, where

The value of ρ can be calculated as [2]

$$\rho = \frac{\sum_{i=2}^n v_i v_{i-1}}{\sum_{i=1}^n v_i^2}. \tag{10}$$

In order to proceed with a normal creep projection with the new model equation (i.e., 6-θ model), it is necessary to know the form of Eq. 2 for all 6-θ parameters. It is not yet established whether these will be of the same form as those currently in use (i.e., a general linear variation with stress and temperature, see Eq. 4). When they are known the projection is carried out in the usual way with certain modifications to take into account the more complex form of Eq. 6 [9]. Some quantities which could previously be found by analytical means may now need some numerical procedures.

Evans [1, 21] has also studied the issue of how to estimate the values for β_i in Eq. 4. OLS works by minimizing the squared deviation between the actual θ_{ij} value and the estimated surface depicted by Eq. 4. If e'_{ij} represent such deviations for a given θ_{ij} then β_0 to β_3 are chosen to minimize $\sum_{j=1}^m e'^2_{ij}$. When this technique is used the resulting 4-θ and 6-θ creep property predictions are said to be unweighted. However, any value obtained for θ_{ij} is only an estimate of its true value and, depending on the nature of the data, some θ_{ij}'s will be estimated with more reliability than others. This reliability is of course measured by the variance associated with each θ_{ij}. This being the case it makes sense to minimise a weighted error sum of squares, $\sum\left(w_{ij} e'^2_{ij}\right)$. Evans (2) has shown that the weights w_{ij} should be given by

$$w_{ij} = \frac{\theta_{ij}^2}{Var\left(\theta_{ij}\right)} \tag{11}$$

where $var(\theta_{ij})$ is the variance associated with the θ_{ij} estimate. This makes sense because the larger is the estimated value for θ_{ij} relative to the uncertainty associated with this estimate, the more influence that estimate should have on the values for β_i. When this technique is used, the resulting 4-θ and 6-θ creep property predictions are said to weighted.

$$v_t = \varepsilon_t - \left\{ \breve{\theta}_1\left[1 - \exp\left(-\overline{\theta}_2 t\right)\right] + \overline{\theta}_3\left[\exp\left(\overline{\theta}_4 t\right) - 1\right] + \overline{\theta}_5\left[1 - \exp\left(-\overline{\theta}_6 t\right)\right] \right\}$$
$$- \rho\left\{ \varepsilon_{t-1} - \left[\overline{\theta}_1(1 - \exp(-\theta_{2t-1})) + \overline{\theta}_3\left(\exp\left(\overline{\theta}_{4t-1}\right) - 1\right) + \overline{\theta}_5(1 - \exp(-\theta_{6t-1}))\right]\right\}. \tag{9}$$

Physical significance of θ parameters

Dependence of power-law creep on the θ parameters

Since full creep curves can be constructed for a material using Eqs. 3 and 4, all features of tradational "power law" behavior such as any creep strain or creep rate parameter can be predicted and explained in a straight forward manner [18]. For example, from Eq. 3, the creep rate at any instant, $\dot{\varepsilon}$, is given by

$$\dot{\varepsilon} = \frac{d\varepsilon}{dt} = \theta_1\theta_2 \exp(-\theta_2 t) + \theta_3\theta_4 \exp(\theta_4 t). \quad (12)$$

Since the rate of change of creep rate is then defined as

$$\frac{d\dot{\varepsilon}}{dt} = \theta_1\theta_2^2 \exp(-\theta_2 t) + \theta_3\theta_4^2 \exp(\theta_4 t). \quad (13)$$

For normal creep curves, a minimum creep rate occurs after a time, t_m, given by

$$t_m = \frac{1}{\theta_2 + \theta_4} \ln\left(\frac{\theta_1\theta_2^2}{\theta_3\theta_4^2}\right) \quad (14)$$

indicating that Eq. 12 has a minimum gradient at the time t_m. For example, the minimum creep rate can then be determined by inserting t_m into Eq. 12 as

$$\dot{\varepsilon}_m = \theta_1\theta_2 \exp(-\theta_2 t_m) + \theta_3\theta_4 \exp(\theta_4 t_m). \quad (15)$$

Therefore, from a knowledge of the values of the 4-θ parameters, t_m and the minimum creep rate, $\dot{\varepsilon}_m$, can be calculated for any stress and temperature. Thus, the θ-projection concept predicts the exact curvature of the experimentally determined $\log\sigma/\log\dot{\varepsilon}_m$ relationships observed even in tests of long duration. Since it is easy to derive the minimum creep rate for various stresses and temperatures, it is also easy to use the θ-data in Eq. 3 to determine the values of n and Q_c at any stress and temperature in a power law relationship:

$$n = \frac{\partial \ln\dot{\varepsilon}}{\partial \ln\sigma} \quad \text{and} \quad Q_c = -R\frac{\partial \ln\dot{\varepsilon}}{\partial(1/T)}. \quad (16)$$

Here n is the stress exponent in power-law creep (PLC), and Q_c the activation energy for creep.

Therefore, without the assumption that different mechanisms become predominant in different stress/temperature regimes [7], all features of tradational power law representation of "steady- state" behavior are simply manifastations of the variations in creep curve shape with stress and temperature, a fact which can now be described quantitatively using the θ-projection concept [6, 8].

Internal structural variable theory: hardening, recovery, and creep damage

Evans [22] has recently derived a constitutive creep model for particle-resistant alloys. It incorporates a variety of physical processes including, hardening, recovery, and damage. For constant stress and temperature, the model yields creep curves which correspond to the θ projection method description of creep, so that the constitutive model can use the extensive experimental data available in the θ method. The internal variables associated with overall hardening (H), recovery (R), and creep damage (W) are all scalar quantities throughout creep life for the alloy. The constitutive equations are

$$\dot{\varepsilon} = \dot{\varepsilon}^o(1 + H + R + W) \quad (17)$$

and

$$\dot{H} = -\widehat{H}\dot{\varepsilon} \quad (18a)$$

$$\dot{R} = \widehat{R} \quad (18b)$$

$$\dot{W} = \widehat{W}\dot{\varepsilon}. \quad (18c)$$

In these equations, $\widehat{H}$, $\widehat{R}$, and $\widehat{W}$ are positive quantities and are functions of stress and temperature. $\widehat{R}$ and $\widehat{H}$ are not the same quantities as those used by Cottrell and Aytekin [23] for recovery rate ($\dot{R}$) and work-hardening rate ($\dot{H}$). $\dot{R}$ and $\dot{H}$ refer to changes in flow stress, whereas $\widehat{R}$ and $\widehat{H}$ govern changes in creep rate. However, since $\widehat{H} = -\dot{H}(\partial\Phi/\partial\sigma)$ and $\widehat{R} = -\dot{R}(\partial\Phi/\partial\sigma)$, then $\widehat{R}/\widehat{H}$ and $\dot{R}/\dot{H}$ are the same and equal to the steady-state creep rate. The creep function Φ depends upon the stress, temperature and internal variables.

Using the constitutive Eqs. 17 and 18, Evans [22] has obtained the creep curve shape equation from zero time up to time t for constant stress and temperature as follows

$$\bar{\varepsilon} = \frac{1}{\widehat{H}\dot{\varepsilon}^o}\left(\dot{\varepsilon}^o - \frac{\widehat{R}}{\widehat{H}}\right)\left(1 - e^{-\widehat{H}\dot{\varepsilon}t}\right) + \frac{1}{\widehat{W}}\left(e^{\left(\widehat{W}\widehat{R}/\widehat{R}\right)t} - 1\right). \quad (19)$$

Equation 19 is exactly the same form as the widely used θ creep curve shape function (see Eq. 3), with the replacement of ε by $\bar{\varepsilon}$ incorporating the known good fit of the equation in complex stress states [24]. Therefore, as determined by Evans [22], it is possible to identify the constitutive equation coefficients $\dot{\varepsilon}^o$, $\widehat{H}$, $\widehat{R}$, and $\widehat{R}$ with the θ coefficients at the same T and σ:

$$\begin{aligned}
\dot{\varepsilon}^o &\equiv \theta_1\theta_2 + \theta_3\theta_4, \\
\widehat{H} &\equiv \frac{\theta_2}{\theta_1\theta_2 + \theta_3\theta_4}, \\
\widehat{R} &\equiv \frac{\theta_2\theta_3\theta_4}{\theta_1\theta_2 + \theta_3\theta_4}, \\
\widehat{W} &= \frac{1}{\theta_3}.
\end{aligned} \quad (20)$$

The above derivations rely on the assumptions outlined concerning the small duration of primary creep. Although

these conditions are met by many particle-hardened alloys, it was not suggested [22] that they apply to all materials irrespective of testing conditions. The assumptions do not remove the appearance of damage from primary creep; both terms in Eq. 19 contain those $\left(\dot{\varepsilon}^o, \widehat{R}, \text{and } \widehat{H}\right)$ which control primary creep.

Therefore, Eqs. 17 and 18, with the constants being determined by Eq. 20, provide a physically reasonable constitutive relationship for structural analysis of particle-hardened alloys where creep is important [22].

Experimental procedure

The material used in this study is a commercial conventionally cast Ni-base superalloy IN-100. The bulk composition of this alloy by wt% is: 10.0 Cr, 15.0 Co, 4.7 Ti, 5.5 Al, 3.0 Mo, 0.18 C, 0.06 Zr, 0.014 B, 1.0 V, and balance nickel. In order to produce a variety of microstructural distributions the creep specimens were deliberately cast to shape at different solidification rates. After casting, the creep specimens were machined to 4-mm gauge diameter. Creep testing was carried out to failure at 1,173 K (900 °C) using a uniaxial constant load in air. Initial stresses ranging from 200 to 400 MPa were applied to creep specimens. The temperature was kept constant within ±0.5 K. The creep elongation was recorded continuously using differential transformers. For the cavity measurements, scanning electron microscope (SEM) cavity micrographs with adjoining fields from the gold-coated samples were taken from the entire cross sections of the fractured specimens. The Cambridge Instruments Q-520 system was used for the quantitative evaluations of cavity size (mean surface area, S), number of cavity per cross section (cavity density, N_A), and cavity volume fraction, f_c. The linear mean cavity size a_c was evaluated as the square root of the mean cavity area (i.e., $S^{1/2}$) whereas the intercavity spacing L, was determined using the following formula: $L = 0.5/N_A^{1/2}$.

Results

θ-Projection concept

Creep curves, obtained under constant-load tests for the initial stresses ranging from 200 to 400 MPa, are normal, i.e., the creep rate decelerates to a minimum before accelerating in tertiary stage. The strain/time readings of each test were obtained from the enlarged creep curves and entered to the computer program in ref. [8] as input. Once the θ values were calculated the complete shape of creep curve can be directly obtained by using Eq. 3. Calculated
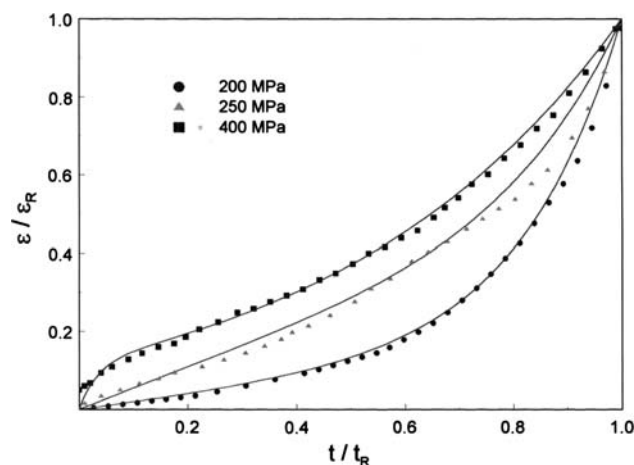

Fig. 1 Creep curves recorded at various initial stresses for conventionally cast IN-100 tested at 900 °C. Actual strain-time readings are given together with the curves obtained using the θ-projection concept

creep strain/time data using θ-projection method together with the observed data are shown in Fig. 1 for selected stresses on normalized axes. It is obvious from these curves that the shape of the creep curves become tertiary dominated with decreasing stress.

The present study has been done at constant temperature therefore only the stress dependence of the creep curves will be quantified through the variation in four θ functions with stress. The variation in four θ functions, calculated using a computer program [8], is presented in Figs. 2 and 3 together with the lines derived for each stress by applying standard linear regression analysis to each set of θ values. The results of regression analysis (standard error being in the range 2.1×10^{-3}–1.3×10^{-4}) are as follows:
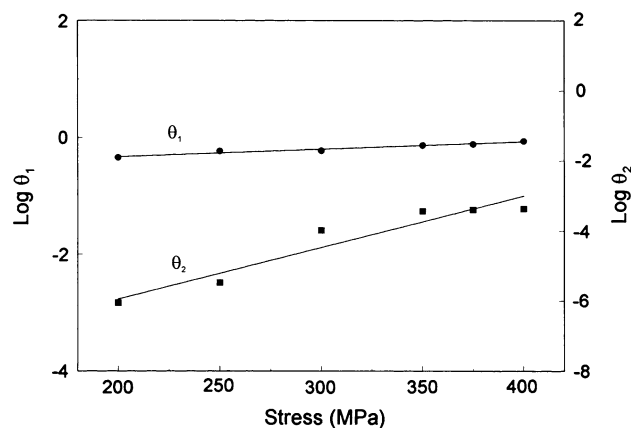
Fig. 2 The stress dependence of parameters θ_1 and θ_2. The values of θ_1 and θ_2 determined from the creep curves obtained at different stresses are shown together with the lines derived by applying standard linear regression analysis to the entire set of θ_1 and θ_2 values
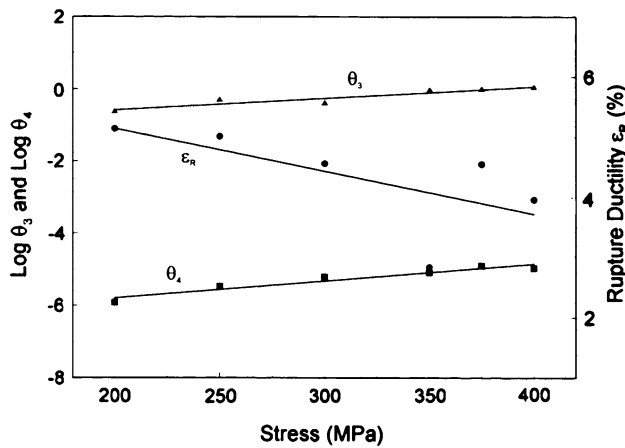
Fig. 3 The stress dependence of parameters θ_3, θ_4, and ε_R. The values of θ_3, θ_4, and ε_R determined for the creep curves obtained at different stresses are shown together with the lines derived by applying standard linear regression analysis to the entire set of θ_3, θ_4, and ε_R values

$$\log \theta_1 = -0.59 + 1.30 \times 10^{-3}\sigma,$$
$$\log \theta_2 = -8.89 + 1.47 \times 10^{-2}\sigma,$$
$$\log \theta_3 = -1.24 + 3.25 \times 10^{-3}\sigma, \qquad (21)$$
$$\log \theta_4 = -6.75 + 4.77 \times 10^{-3}\sigma,$$
$$\varepsilon_R = 6.56 - 7.11 \times 10^{-3}\sigma,$$

where σ is the applied initial stress (σ_A). Rupture ductility ε_R shows a small decrease with increasing applied stress as shown in Fig. 3 together with the predicted values. The result of linear regression analysis (standard error is 4.2×10^{-3}) for rupture ductility is included in Eq. 21 above. Differences between the θ parameters of the present study and previous one [11] for the same superalloy is believed to be due to the application of constant-load test data, in which the stress in the sample gradually increases up to the failure. Although the constant-load test data were used for predictions of θ values and rupture strain, reasonable fits were achieved. It should be emphasized that no attempt has been made for life prediction in the present study, since such predictions will be in error due to severe distortions at high stresses in constant-load test [6].

Fracture cavitation

A quantitative investigation of cavities was carried out on fractured specimens. The nature of cavities taken from positions adjacent to fracture surface for two different samples is shown in Fig. 4. In Fig. 4a, taken from sample tested at 250 MPa, the cavities have larger sizes but they are few comparing to Fig. 4b, which shows the cavitation at 375 MPa. In both SEM micrographs, the cavities are not continuous implying that fracture occurred due to a very rapid linkup of cavities during the last stage of tertiary creep. The relation between applied initial stress and cavity
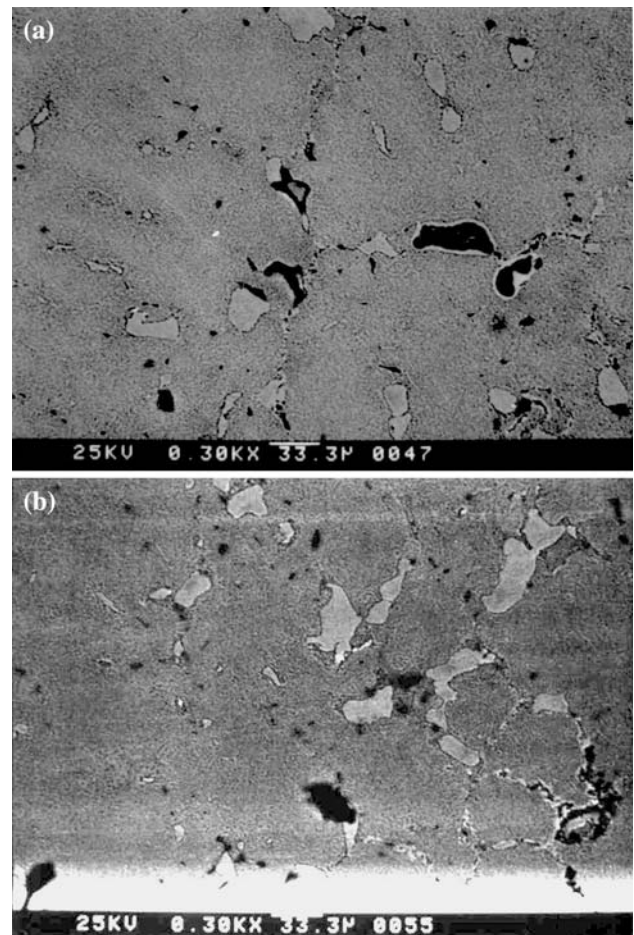
Fig. 4 Different cavity morphologies observed at different stresses. (**a**) Larger sized cavities observed at 250 MPa. (**b**) Smaller sized and numerous cavities observed at 375 MPa
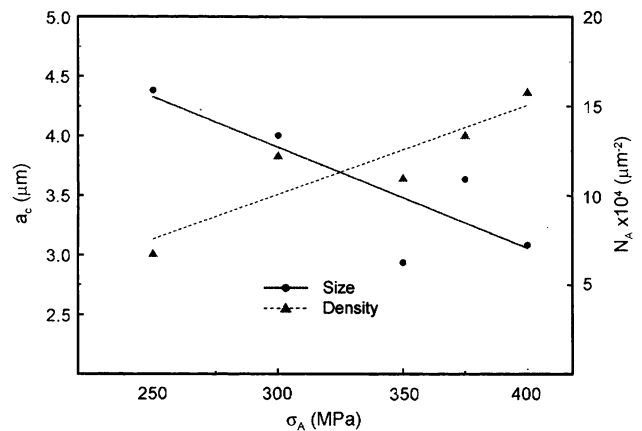

Fig. 5 Variations in cavity size a_c and density N_A with applied initial stress σ_A

parameters (i.e., size and density) is shown in Fig. 5. The decrease in crack size with increase in stress level has been attributed [25] to the fact that crack growth past a grain boundary (GB) carbide particle is difficult.
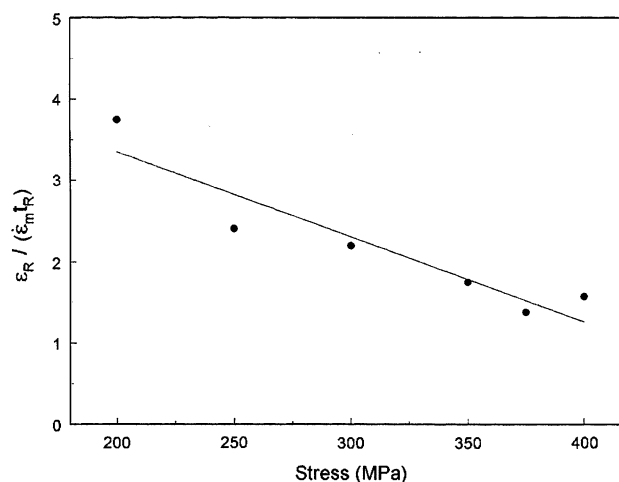
Discussion

Creep damage mechanism

The fracture of metals after high temperature creep results from the progressive accumulation of damage through the creep life. The first indication of eventual fracture is usually the acceleration in creep rate at the onset of tertiary stage of creep. It is reported that [26], the creep damage is generally due to (i) the development of GB cavities and cracks to a size sufficient to affect the deformation processes [27] or (ii) microstructural instability such as grain growth or recrystallization [28] or changes in particle dispersion during the creep of two-phase alloys [29]. A way of distinguishing the creep damage mechanism has been proposed by Ashby and Dyson [30]. They suggested that the creep damage tolerance parameter λ, defined by $\lambda = \varepsilon_R/(\dot{\varepsilon}_m t_R)$, originally introduced by Leckie and Hayhurst [31], could be used to identify the dominant creep mechanism. According to this parameter, failure dominated by GB cavitation tends to occur in the range $1 < \lambda < 2.5$ and failure dominated by microstructural degradation occurs at values of λ around 10 or higher. For the present study, the damage tolerance parameter λ was calculated by plotting $\dot{\varepsilon}_m$ against ε_R/t_R as shown in Fig. 6. From this figure the parameter λ (i.e., the slope of the line) was found to be around 1.34 which lies in the range $1 < \lambda < 2.5$, suggesting that for the present superalloy and creep conditions (200–400 MPa and 900 °C) failure is dominated by GB cavitation. The quantity λ measures the tolerance of the material to strain concentrations. A large λ means that the material can tolerate the strain concentrations without local cracking [30]. But for the present superalloy this quantity is low, implying that the cracks started to initiate at strain
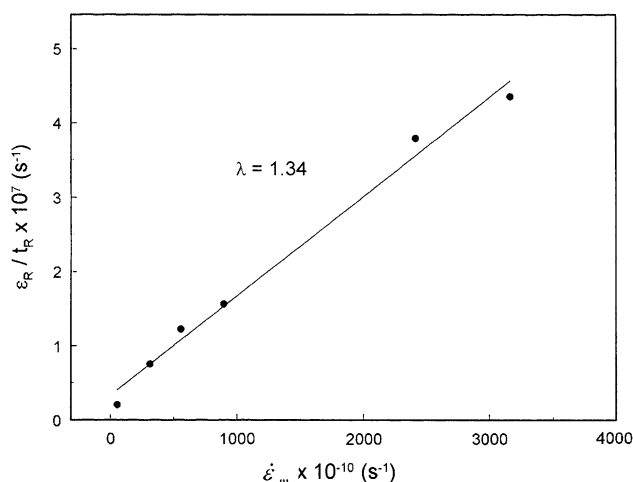
Fig. 7 Variation in damage tolerance parameter λ with applied initial stress σ_A

concentrations (i.e., at cavities and carbide particles on grain boundaries). This situation is more pronounced at higher stresses as shown in Fig. 7. At higher stresses the plastic flow of material and therefore strain accumulation is rapid, causing the strain to concentrate and eventually leading the formation of cavities at discontinuities on grain boundaries. Numerous and small sized cavities observed at 375 MPa (see Figs. 4b and 5) support this view.

Failure by GB cavitation includes several sequential processes such as nucleation and growth of cavities, coalescence of cavities into cracks and the interlinkage of microcracks to form a macroscopic crack across the components leading to final fracture. Among these processes cavity growth is usually the rate-controlling step and has been studied extensively in the past. Cavities grow by mechanisms controlled by GB diffusion, by surface diffusion, by PLC or by any combination of two of these mechanisms. Needleman and Rice [32] introduced a stress and temperature-dependent characteristic diffusion length, Λ:

$$\Lambda = \left(\frac{D_B \delta_B \Omega \sigma_\infty}{kT\dot{\varepsilon}_\infty}\right)^{1/3}, \tag{22}$$

where D_B (m^2 s^{-1}) is the GB diffusion coefficient, δ_B (m) the GB width, Ω (m^3) the atomic volume, σ_∞ (MNm^{-2}) the remotely applied stress (or σ_A), k the Boltzmann's constant (1.38×10^{-23} JK^{-1}), T the absolute temperature and $\dot{\varepsilon}_\infty$ the remote creep rate (or minimum creep rate, $\dot{\varepsilon}_m$). The contribution of dislocation creep (i.e., PLC) to cavity growth is shown to be negligible when $\Lambda > L$ and significant interaction occurs when $\Lambda < L$.

Edward and Ashby [33] determined the size of the diffusional zone by a dimensionless parameter P^*:

Fig. 6 Calculation of damage tolerance parameter, defined by $\lambda = \varepsilon_R/(\dot{\varepsilon}_m t_R)$. The slope of the straight line is $\lambda \approx 1.34$

$$P^* = \frac{1}{10}\left[2\Phi_o'\left(\frac{\sigma_o}{\sigma_1}\right)^{n-1}\right]^{2/n}, \qquad (23)$$

where σ_0 (MNm^{-2}) is the creep constant, σ_1 (MNm^{-2}) is the principle stress, n the stress exponent. Φ_0' is defined [34] as the important material property by,

$$\Phi_o' = \beta f_c^{1/2}\ln\left(\frac{1}{f_c}\right)\left[\frac{1}{(1-f_c)^n} - (1-f_c)\right]\left(\frac{\sigma_e}{\sigma_o}\right)^n\frac{\sigma_o}{\sigma_1}, \qquad (24)$$

where β is a constant, f_c the cavity volume fraction, and σ_e the equivalent tensile stress. For simple tension $\beta = 0.6$ and $\sigma_e = \sigma_1$ [34]. For polycrystalline materials σ_1 may be taken to be equal to σ_A. The parameter P^* is also useful for the determination of which mode of cavity growth mechanism dominates the creep life under various conditions. It was predicted that [33] for $P^* > 1$ the diffusion fields of the cavities overlap and PLC can be ignored. When $P^* < 10^{-3}$ diffusion is negligible and PLC is dominant. Within the above two bounds of P^* ($10^{-3} < P^* < 1$), both the diffusion and the PLC growth contributions are important in determining the creep rupture life t_R. Using the following material constants [25] for the present Ni-base superalloy, the parameters Λ, Φ_0', and P^* were calculated for various σ_A, f_c, L, and $\dot{\varepsilon}_m$ values observed in the present investigation.

$\delta_{OB}D_{OB} = 2.8 \times 10^{-15}\,\text{m}^3\text{s}^{-1}$,
$\Omega = 1.1 \times 10^{-29}\,\text{m}^3$,
$Q_B = 115\,\text{kJ mol}^{-1}$,
$\beta = 0.6$ for simple tension
$\sigma_o = 4{,}097$ MPa,
$n = 5$ (stress exponent for present study),

where $\delta_{OB}D_{OB}$ is the pre-exponential term for the GB diffusion constant, Q_B is the activation energy for GB diffusion. Note that $\delta_B D_B$ was calculated using the following Arrhenius type equation [35].

$$\delta_B D_B = \delta_{OB}D_{OB}\exp\left(-\frac{Q_B}{RT}\right) \qquad (25)$$

with R the gas constant ($8.31\,\text{Jmol}^{-1}\text{K}^{-1}$). The calculated values of Λ, L, Φ_0' and P^* for the present creep conditions ($T = 900\ ^\circ\text{C}$ and $\sigma_A = 200$–400 MPa) are given in Table 1.

Table 1 Calculated parameters Λ, Φ_0', and P^* for various σ_A, L, and $\dot{\varepsilon}_m$ values using Eqs. 22, 24 and 23, respectively

σ_A (MPa)	Λ (μm)	L (μm)	$\Phi_o' \times 10^6$	P^*
200	80.4	10.2	0.37	0.134
250	48.5	19.3	1.34	0.157
300	42.6	14.3	2.67	0.155
350	38.3	15.1	4.61	0.150

These numerical calculations suggest that the creep fracture cavity growth is controlled by the coupled GB diffusion with PLC mechanism (i.e., $\Lambda > L$ and $1 > P^* > 10^{-3}$). For this coupled mechanism under constant-load conditions, an approximate analytical equation for the rupture life t_R is given [34] as,

$$t_R = t_n + \frac{2}{3}\frac{(f_t^b)^{3/2}}{\Phi_o'\dot{\varepsilon}_o}\left[\ln\left(\frac{1}{f_t^b}\right) + \frac{2}{3}\right]\frac{\sigma_o}{\sigma_1} + \frac{1}{[\beta(n+1)\dot{\varepsilon}_o]}\ln\left[\frac{1}{(n+1)f_t^b}\right]\left(\frac{\sigma_o}{\sigma_e}\right)^n, \qquad (26)$$

where $\dot{\varepsilon}_0(\text{s}^{-1})$ is the creep constant, f_t^b the area fraction of cavity holes at transition from growth by GB diffusion to PLC growth in approximate analysis and is given by

$$f_t^b = \frac{1}{[d(\ln d - 1)]^{3/2}}, \qquad (27)$$

where,

$$d = \frac{4(n+1)\sigma_o\beta}{3\Phi_o'\sigma_1}\left(\frac{\sigma_e}{\sigma_o}\right)^n. \qquad (28)$$

Neglecting all the constant parameters except σ_0 and assuming that t_n is very small quantity, Eq. 26 reduces to,

$$t_R \propto \frac{(f_t^b)^{3/2}}{\Phi_o'}\ln\left(\frac{1}{f_t^b}\right)\left(\frac{\sigma_o}{\sigma_1}\right) + \ln\left(\frac{1}{f_t^b}\right)\left(\frac{\sigma_o}{\sigma_e}\right)^n = A. \qquad (29)$$

Our aim is to check whether the growth mechanism is the coupled GB diffusion with PLC, not to predict the exact rupture life. Therefore a linear relation between the observed rupture life and *parameter A* will verify the estimated coupled growth mechanism. The *parameter A*, calculated using Eq. 29, was plotted against the observed rupture life t_R as depicted in Fig. 8. The linear relationship
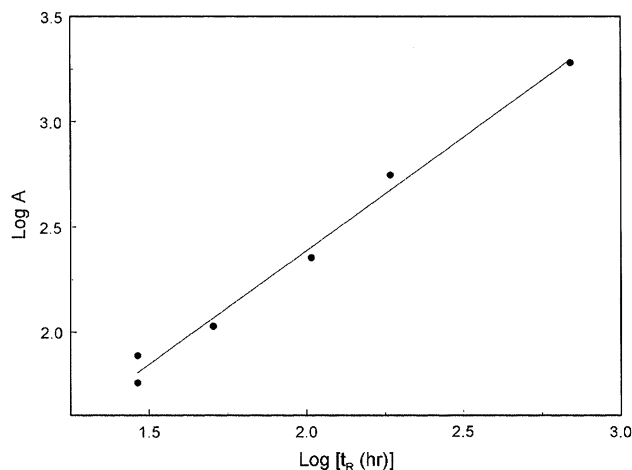
Fig. 8 The linear relationship between the observed creep rupture life t_R for various initial stresses and parameter A calculated using Eq. 10

between *parameter A* and observed rupture life in this figure implies that the prediction of dominant cavity growth mechanism (i.e., coupled GB diffusion with PLC) is applicable.

Creep deformation and creep curve shape

The creep behavior of present superalloy at constant temperature can be described using a power–law relationship of the form,

$$\dot{\varepsilon}_m = C_1 \sigma^{n_1}, \tag{30a}$$

$$t_R = C_2 \sigma^{-n_2}, \tag{30b}$$

where C_1, C_2, n_1, and n_2 are constants. The stress dependence of minimum creep rate and rupture life are shown together in Fig. 9, which gives the apparent stress exponents as $n_1 = 5.4$ and $n_2 = 4.6$. The similar dependence of $\dot{\varepsilon}_m$ and t_R on applied stress suggest that the rate of development of cracks is somehow related to deformation processes. The shape of the creep curve changes with applied stress. As depicted in Fig. 1 while the shape of the creep curve is tertiary dominated at 200 MPa, a discernible primary region becomes apparent at 400 MPa. In other words, tertiary creep commences in an early fraction of creep life with longer test durations which results reduced t_s/t_R ratios (t_s is the time to commencement of tertiary creep) at low stresses as shown in Fig. 10.

In theta projection concept a normal creep curve is envisaged as the sum of a decaying primary and an accelerating tertiary component. Equivalently, total creep strain (i.e., rupture strain) and total creep life (i.e., rupture life) can be thought of consisting of two components, namely primary and tertiary components since the secondary creep region is considered as the period of
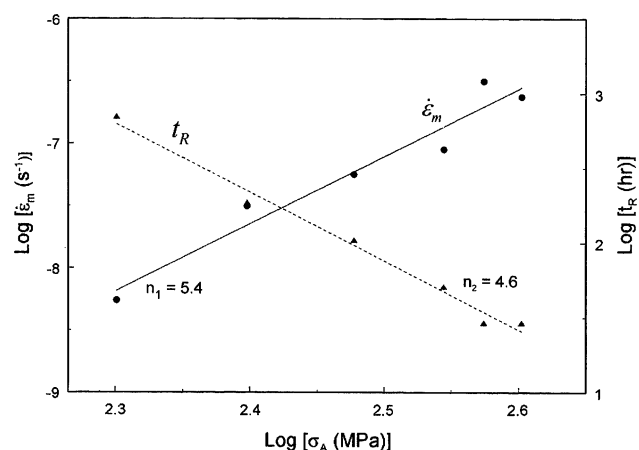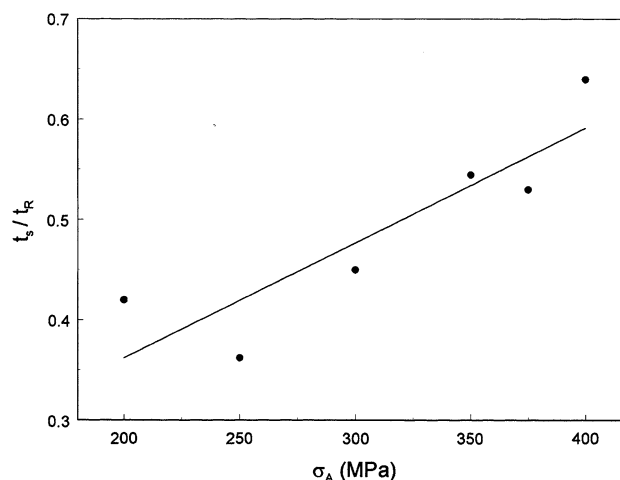
Fig. 10 Variation in t_s/t_R (the ratio of time to the commencement of tertiary creep, t_s to the rupture life, t_R) with applied initial stress σ_A

inflection between primary and tertiary components. At low stresses ($\sigma < 250$ MPa) the creep rate is almost continuously increasing giving a tertiary dominance to the curve shape. But with increasing stress the period of inflection, over which the creep rate is almost constant, becomes apparent and the fraction of strain in the secondary region (ε_m) to overall creep strain increases. Distinguishable secondary creep region with increased stress is believed to be a result of constant-load test, as the stress in the sample increases gradually with time giving a steeper view to the creep curve shape. Moreover, the fraction of primary creep strain ε_p^* (strain from the beginning up to the onset of secondary creep) to overall strain increases with stress while the fraction of tertiary creep strain ε_t^* (strain from the onset of tertiary creep up to the failure point) to overall strain decreases. In order to be able to compare the observed primary and tertiary components of strain with those calculated from Eq. 3, total creep strain observed in the present study has been separated into two components. The primary strain ε_p is the same as defined above ($\varepsilon_p = \varepsilon_p^*$) but the tertiary strain ε_t, in this case is the strain from the onset of secondary creep up to the failure point, i.e., the strain corresponding to secondary creep has been added to ε_t^* ($\varepsilon_t = \varepsilon_m + \varepsilon_t^*$ and $\varepsilon_R = \varepsilon_p + \varepsilon_t$). The stress dependence of the observed strain components together with the calculated ones are shown in Fig. 11, which provides more evidence that the shape of the creep curve changes from tertiary dominant to primary dominant appearance. Although there is a discernible secondary creep region at higher stresses, the predictions made by using θ-projection concept are reasonable enough showing the high prediction capability of this empirical approach even at constant-load tests.

Fig. 9 Stress dependence of the minimum creep rate $\dot{\varepsilon}_m$ and the rupture life t_R
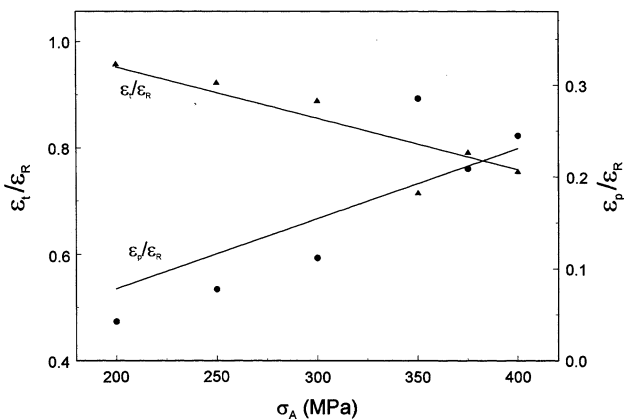
Fig. 11 Variations in strain components (ε_p and ε_t) with applied initial stress σ_A. Observed values (symbols) of ε_p (strain from the beginning up to the onset of secondary creep) and ε_t (strain from the onset of secondary creep up to the failure) are shown together with the calculated values (lines) using θ-projection concept

Primary and tertiary creep processes

In predicting cavity-growth mechanism, although the nucleation time for cavities t_n was assumed to be a very small quantity, it is evident from the SEM micrographs, taken from the fractured specimens, that there are numerous cavities having very small sizes (Fig. 4a, b), which are thought to be an indication of continuous cavitation, i.e., t_n is large. This situation has been observed at all stress levels. The fact that t_n is not a negligible quantity does not alter the prediction that cavity growth is controlled by the coupled GB diffusion and PLC mechanism. Because of continuous cavitation, it is expected for the cavities to attain larger sizes at higher ductilities as shown in Fig. 12, together with the calculated rupture ductilities. For the
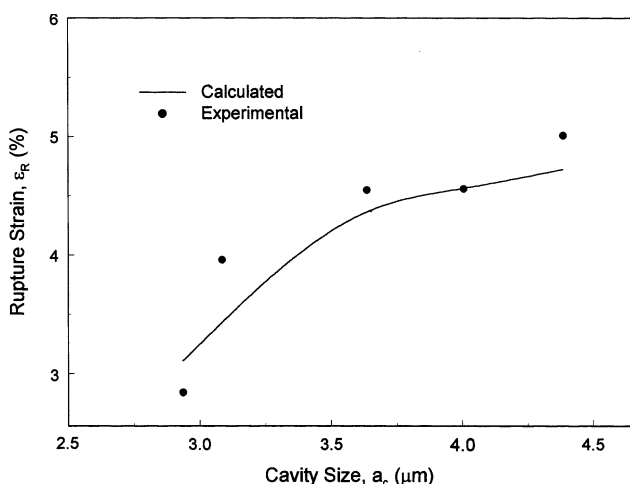
Fig. 12 Variation in rupture ductility ε_R with mean cavity size a_c. Observed values (symbols) of rupture ductility are shown together with the calculated values (line) using θ-projection concept

present study, it was predicted with parameter λ that failure is dominated by GB cavitation, therefore it is suggested that the acceleration in creep rate during the tertiary stage is a consequence of intergranular damage processes which are controlled by the rate of deformation (Fig. 9), i.e., the development of GB cracking is strain controlled.

The change in stress exponent n and activation energy for creep Q_c are generally explained by the change in creep deformation mechanisms at different stress and temperature regimes. It has been shown in detail [6, 8, 11, 16] that the changes in n and Q_c are the result of the variations in creep curve shape with stress and temperature, which satisfactorily quantified by θ-projection concept. Therefore, it seems that there must be a relationship between processes responsible for the deformation in primary and/or tertiary regions and theta parameters.

As it was stated before, the creep strain in Eq. 3 is the sum of two terms, the first representing decaying primary (ε_p) and the second accelerating tertiary (ε_t). These strain components and their derivatives (strain rates) can be written as [8];

$$\varepsilon_p = \theta_1[1 - \exp(-\theta_2 t)], \tag{31}$$

$$\frac{d\varepsilon_p}{dt} = \theta_2(\theta_1 - \varepsilon_p), \tag{32}$$

$$\varepsilon_t = \theta_3[\exp(\theta_4 t) - 1], \tag{33}$$

$$\frac{d\varepsilon_t}{dt} = \theta_4(\theta_3 + \varepsilon_t). \tag{34}$$

It is clear from the strain-rate equations above that the kinetics of the primary and tertiary processes are both first order and this must be recognized in any mechanism proposed to account for the theta description of the creep curve. There are a number of possible mechanisms [8] and it is necessary to test their practical kinetics against Eqs. 31–34.

Primary creep process

Previously proposed models that include different processes that can give rise to a creep rate, which decays with time, namely those which involve the exhaustion of deformation elements [36] and those which consider work hardening to be dominant feature [20, 37], ignored the effects of recovery processes. On the other hand, the internal structure variable theory proposed by Nix et al. [20, 38] is of sufficient generality to allow an analysis in terms of θ primary creep equation (Eq. 31). According to this theory the creeping material is divided into two regions, hard and soft regions. Screw dislocations move readily in cell interiors (soft regions) but their edge components collect in the cell walls (hard regions). With this theory, two equations were developed for each sub-region,

the kinetic equation and the growth equation, which have the same general form in all regions. Evans and Wilshire [8] have considered this theory as one of the possible mechanism and tried to correlate it with θ primary equation. They derived the kinetic equation, combining with the growth equation and concluded that the creep strain for an individual sub-region has the form;

$$\varepsilon = \frac{kT}{BbA^*\alpha}\left[B - \frac{\beta}{\alpha}\right]\left[1 - \exp\left(-\frac{BbA^*\alpha}{kT}t\right)\right] + \frac{\beta}{\alpha}t, \quad (35)$$

where B represents the strain-rate at zero time, k the Boltzmann's constant, T the temperature, b the Burger's vector, A^* the activation area, and α and β represent a measure of strain hardening rate and recovery rate, respectively. The first term in above equation has the same form as the θ equations for primary creep. The term corresponding to θ_1 will have a temperature sensitivity governed largely by the ratio β/B and since β represents recovery rate the temperature sensitivity will reside mainly in the variation of A^* and α. Thus it is to be expected that θ_1 would scale reasonably with the general temperature dependence of plastic properties, such as plastic yield stress. But the present study has been carried out at constant temperature and it is not possible here to test the temperature dependence of θ_1 against plastic properties, nevertheless it has been shown for different materials [8, 11, 16, 17] that θ_1 scales reasonably when it is superimposed by normalizing the applied stress in terms of the plastic yield stress, i.e., the extent of the total primary strain has a temperature dependence identical with that of yield stress.

On the other hand, the term representing θ_2 ($= \alpha b A^* B/kT$) will have a temperature and stress sensitivity close to that of B which will have an activation energy near to the creep process (and often equal to that of self-diffusion). For the present work assuming that the creeping specimen is a single region and that A^* is constant (b, k, and T constant) we have,

$$\theta_2 \propto \alpha B. \quad (36)$$

The strain-hardening rate can be estimated from the recovery theory proposed by McLean [39] and refined by Lagneborg [40]. The local stress σ, at the three dimensional network is related to the mesh size and hence ρ, where ρ is the dislocation density. Since σ is proportional to $Gb\rho^{1/2}$, G is the shear modulus, and ρ is also proportional to the creep strain ε,

$$\alpha = \frac{\partial\sigma}{\partial\varepsilon} \propto \frac{1}{\sigma}. \quad (37)$$

Substituting α into Eq. 36,

$$\theta_2 \propto \frac{B}{\sigma}. \quad (38)$$
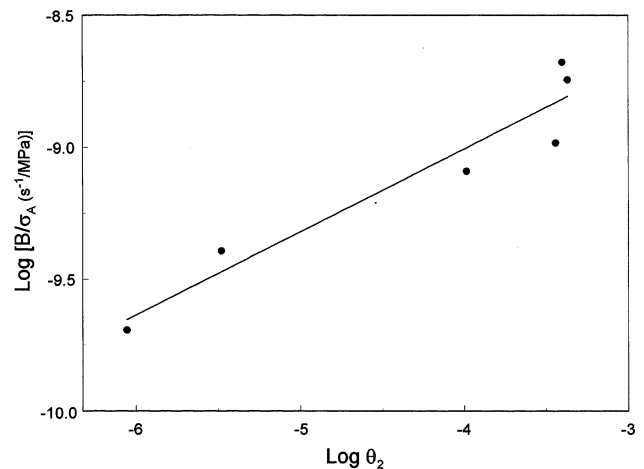
Fig. 13 The linear relationship between the rate constant characterizing the shape of the primary creep curve (θ_2) and parameter B/σ, i.e., Eq. 19

Strain rate at zero time (B) has been calculated from experimental creep curves by using first two data points right after the instantaneous strain. Equation 38 has been plotted on a log–log scale as shown in Fig. 13 in which illustrates a reasonably good linear relationship between θ_2 and B/σ and indicates the first-order kinetics of primary creep described by Eq. 32. The linear correlation between rate constant θ_2 and B/σ implies that the internal structure variable theory [20, 38] accounts well for the θ description of the primary creep curve.

Tertiary creep process

A common cause of degradation during creep is the nucleation and growth of GB cavities. In the section "creep damage mechanism" it was predicted that the failure is dominated by the GB cavitation ($1 < \lambda < 2.5$). Furthermore it was also observed from SEM micrographs (Fig. 4a, b) that there is a continuous cavitation during the course of creep deformation. In several cases it has been shown that [41, 42] the volume of GB cavities increases approximately linearly with strain, so that the description of tertiary creep contained in Eq. 34 implies that creep strain rate is proportional to void volume. A direct dependence of the tertiary strain on void volume would be expected from a model for tertiary creep [43] based on the cavity growth by absorption of vacancies from the surrounding GB, which is equivalent to plating out of atoms on boundaries perpendicular to the applied stress, thereby achieving creep strain in a direction parallel to the stress axis.

In the present case, only the size and hence the volume of cavities at fracture have been measured and not at the intermediate stages during creep deformation. Therefore the proportionality between creep strain/strain rate and void
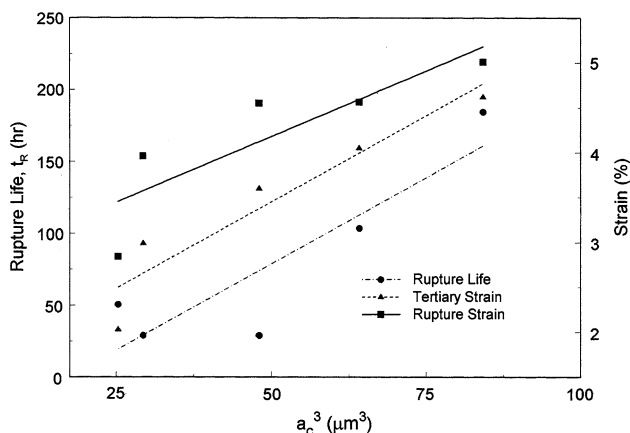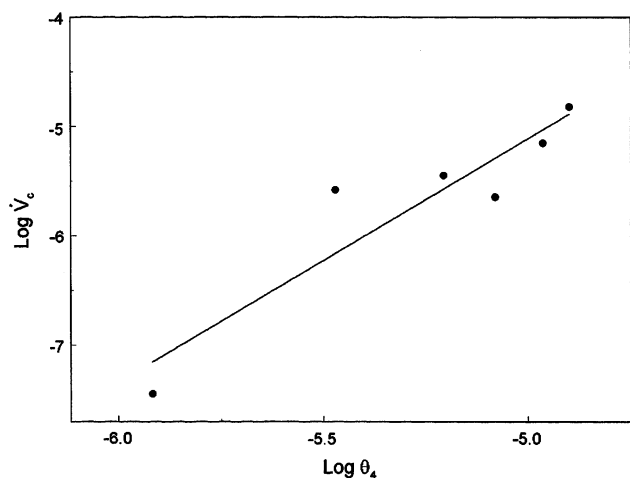
Fig. 14 The linear relationships between cavity volume at fracture (V_c) and rupture life t_R, rupture ductility ε_R and tertiary strain ε_t

volume cannot be tested, instead probable linear relationship between void volume at fracture and rupture life (or rupture ductility) can be determined. Consequently, it is concluded that a linear relationship between void volume and tertiary strain or rupture life (or rupture ductility) will imply that GB cavitation account for the θ description of the tertiary creep curve. Volume of a cavity can be written as,

$$V_c \propto a_c^3. \qquad (39)$$

The expected linear relationship between cavity volume at fracture and tertiary strain, rupture life and rupture ductility are shown in Fig. 14, which confirms the above conclusion and shows the fact that creep rupture properties (ε_R and t_R) for the present superalloy are directly controlled by the GB cavitation process. The rate of void volume enlargement, $\dot{V}_c$ is given [32] to be,

$$\dot{V}_c \propto \dot{\varepsilon}_\infty a_c^3. \qquad (40)$$

Fig. 15 The linear relationship between the rate constant characterizing the shape of the tertiary creep curve (θ_4) and the volumetric growth rate of cavities ($\dot{V}_c$)

Further support to the above conclusion can be provided by the graph of Log θ_4 vs. Log$\dot{V}_c$ as shown in Fig. 15, in which the rate parameter that characterizes the curvature of the tertiary creep, θ_4, is linearly proportional to the cavity volumetric growth rate, $\dot{V}_c$. It is suggested that both figures (Figs. 14 and 15) provide physical basis for the θ description of the tertiary creep.

Concluding remarks

The empirical approach, termed θ-projection concept, is applied to constant-load test data of conventionally cast Ni-base superalloy IN-100. Similar work has been carried out in the past [11], but for constant-stress data. It has been reported that [6], the difference in testing methods affects greatly the creep behavior by altering the rupture life and entire curve shape. Change in entire creep curve shape directly changes the θ parameters, which in turn may change the deformation behavior, especially in short-term tests where stress intensification is severe and leads to much reduced life. Therefore, the difference between either θ parameters or deformation mechanisms predicted for the present study and that of in the past [11] can be attributed to the different testing methods.

The normal creep curves, obtained at various initial stresses, could be accurately represented by using Eq. 3 (Fig. 1). It is predicted that failure is dominated by the GB cavitation and the growth of GB cavities controlled by the coupled mechanisms of GB diffusion and PLC. The exponents in the power–law relationship of minimum creep rate and rupture life with stress (Eq. 30) are similar suggesting that creep rupture process in the tertiary creep region is somehow related to the deformation process in the secondary region. It is also found that, the shape of the creep curve changes from tertiary dominant to primary dominant view with increasing stress, i.e., the commencement of tertiary creep occurs progressively earlier fraction of the rupture life as the stress is decreased. In an attempt to establish a physical significance of the θ parameters employed, it is found that *internal structural variable theory* [20, 38] accounts well (with suitable assumptions) for the θ description of the primary creep curve (Fig. 13). The indication of continuous cavitation from SEM micrographs supports the prediction that failure is dominated by GB cavitation. Increased cavity volume with a linear increase in tertiary strain, rupture life and rupture ductility provides a physical meaning to the θ description of tertiary creep curve (Fig. 14). Eventually, it is suggested that, empirical θ-projection concept can be used with greater confidence since it is supported by a physical understanding of the concepts involved for the present creep conditions.

References

1. Evans M (2000) J Strain Anal 35:389
2. Evans RW (1989) Mater Sci Technol 5:699–707
3. Larson FR, Miller J (1952) Trans ASME 74:756
4. Orr RL, Sherby OD, Dorn JE (1945) Trans ASM 46:113
5. Manson SS, Haferd AM (1953) NACA. TN 2890, March
6. Evans RW, Parker JD, Wilshire B (1982) In: Wilshire B, Owen DRJ (eds) Recent advances in creep and fracture of engineering materials and structures. Pineridge Press, Swansea, Swansea, p 135
7. Wilshire B (1989) New lamp's for old. In: Taplin DMR, Knott JF, Lewis MH (eds) Second Parsons International Turbine Conference on the "Materials Development in Turbo-Machinary Design". The Institute of Metals, London, Parsons Press, Trinity College, Dublin, pp 263–268
8. Evans RW, Wilshire B (1985) Creep of metals and alloys. The Institute of Metals, London
9. Evans RW (2000) Mater Sci Technol 16:6
10. Beden I, Brown SGR, Evans RW, Wilshire B (1987) Res Mech 22:45
11. Evans RW, Brown SGR, Wilshire B (1986) Mater Sci Eng 84:147
12. Evans RW, Scharning PJ, Wilshire B (1985) In: Wilshire B, Evans RW (eds) Creep behaviour of crystalline solids. Pineridge Press, Swansea, p 201
13. Evans RW, Murakami T, Wilshire B (1988) Trans J Br Ceram Soc 87:54
14. Li G, Sakai T, Endo T (1987) An Application of Creep Time Law to the Life Prediction of a Nickel-Base Superalloy. In: Proceedings of the Third International Conference on the "Creep and Fracture of Engineering Materials and Structures", held at University College, Swansea, 5–10 April, 1987, pp 803–813
15. Frost HJ, Ashby MF (1982) Deformation-mechanism maps. Pergamon Press, Oxford, p 1
16. Brown SGR, Evans RW, Wilshire B (1987) Mater Sci Technol 3:23
17. Evans RW, Fadlalla AA, Wilshire B (1990) In: Wilshire B, Evans RW (eds) Proceedings of the 4th international conference on "Creep and Fracture of Engineering Materials and Structures". Swansea, The Institute of Materials, London, p 1009
18. Evans RW, Wilshire B (1987) Power law creep of polycrystalline copper. In: Wilshire B, Evans RW (eds) Proceedings of the Third International Conference on "Creep and Fracture of Engineering Materials and Structures" held at University College, Swansea, UK, 5–10 April 1987. Inst. of Metals, London, pp 59–70
19. Evans RW, Wilshire B (1987) Mater Sci Technol 3:701
20. Nix WD, Gibling JC (1983) Mechanisms of time dependent flow and fracture. The American Society for Metals, Metals Park
21. Evans M (2000) J Mater Sci 35:2937
22. Evans RW (2000) Proc R Soc Lond A 436:835
23. Cottrell AH, Aytekin V (1950) JIM 77:389
24. Evans RW, Wilshire B (1996) In: Krausz AS, Krauss K (eds) Unified constitutive laws of deformation. Academic Press, p 108
25. Baldan A (1998) J Mater Sci 33:3629
26. Baldan A (1991) J Mater Sci 26:3409
27. Perry AJ (1974) J Mater Sci 9:1016
28. Dennison JP, Wilshire B (1962) J Inst Metals 91:343
29. Williams KR, Wilshire B (1977) Mater Sci Eng 28:289
30. Ashby MF, Dyson BF (1984) In: Valluri SR, Taplin DMR, Rama Rao P, Knott JF, Dubey R (eds) Proceedings of the 6th international conference on fracture (ICF6), New Delhi, India, vol 1. Pergamon Press, Exeter, p 3
31. Leckie FA, Hayhurst DR (1977) Acta Metall 25:1059
32. Needleman A, Rice JR (1980) Acta Metall 28:1315
33. Edward GH, Ashby MF (1979) Acta Metall 27:1505
34. Cocks ACF, Ashby MF (1982) Progr Mater Sci 27:189
35. Frost HJ, Ashby MF (1982) Deformation mechanism maps, the plasticity and creep of metals and ceramics. Pergamon Press, Oxford, p 55
36. Mott NF, Nabarro FRN (1948) Strength of solids. Physical Society, London, p 1
37. Mott NF (1953) Phil Mag 44:742
38. Nix WD, Ilschner B (1979) In: Haasen P, Gerold V, Kostorz G (eds) Proceedings of the 5th international conference on strength of metals and alloys ICMA5, Aachen, vol 3. Pergamon Press, Oxford, p 1503
39. McLean D (1966) Rep Prog Phys 29:1
40. Lagneborg R (1969) Met Sci J 3:161
41. Boettner RC, Robertson WD (1961) Trans AIME 221:613
42. Bowring P, Davies PW, Wilshire B (1968) Metal Sci J 2:168
43. Harris JE, Tucker MO, Greenwood GW (1974) Metal Sci 8:311